https://doi.org/10.2478/acph-2025-0009

Original research paper

FOXD2-AS1 is modulated by METTL3 with assistance of YTHDF1 to affect proliferation and apoptosis in esophageal cancer

ZI JIN WANG
XING CHEN LIU
ZHEN GYA GAO
WO DA SHI*
WEN CAI WANG*

Department of Cardiothoracic Surgery, Affiliated Hospital 6 of Nantong University，The Yancheng School of Clinical Medicine of Nanjing Medical University, Yancheng Third People's Hospital，Yancheng，Jiangsu，224000 China

ABSTRACT

This study aims to investigate the regulatory mechanisms of METTL3, YTHDF1, and the long non-coding RNA FOXD2-AS1 in the proliferation and apoptosis of esophageal cancer, with the goal of providing a basis for molecular diagnosis and targeted therapies. Gene expression was evaluated using qRT-PCR (METTL3/14) and Western blot analysis. The Cell Counting Kit-8 (CCK-8) assay, flow cytometry, and Transwell assay were employed to assess cell proliferation and apoptosis. The EpiQuik m6A RNA Methylation Quantification Kit was utilized to quantify total m6A levels. The interaction between YTHDF1, FOXD2-AS1, and METTL3 was confirmed using RNA Binding Protein Immunoprecipitation (RIP), Co-Immunoprecipitation (CO-IP), and RNA pull-down assays. Methylated RNA Immunoprecipitation (MeRIP) was employed to assess the m6A modification levels of FOXD2-AS1. Tissue samples from animal models were analyzed via Hematoxylin-eosin staining (HE) staining and immunohistochemistry to assess METTL3 expression.

The expression of *METTL3* was up-regulated in esophageal cancer tissues and cells. Flow cytometry and CCK-8 detection showed that silencing *METTL3* could inhibit the proliferation of esophageal cancer cells but accelerate their apoptosis. MeRIP-qPCR and Prediction of m6A-modified sites indicated that METTL3 regulated the m6A modification of FOXD2-AS1. *In vitro* and *in vivo* experiments showed that YTHDF1 binds to METTL3 and regulates the m6A modification of FOXD2-AS1 to affect esophageal cancer. Our results indicate that METTL3 regulates FOXD2-AS1 in an m6A-dependent manner through its interaction with YTHDF1, thereby influencing EC proliferation and apoptosis. This suggests a potential therapeutic target for the treatment of esophageal cancer.

Keywords: esophageal cancer, FOXD2-AS1, METTL3, YTHDF1

Accepted March 19, 2025
Published online March 20, 2025

* Correspondence, e-mail: wangwencai1949@sina.com

INTRODUCTION

Esophageal cancer (EC), which includes esophageal squamous cell carcinoma (ESCC; 90 %) and esophageal adenocarcinoma (EAC), is a major contributor to cancer-related mortality, primarily due to the advanced stage at diagnosis and limited treatment efficacy (1, 2). Its aggressive nature, coupled with an increasing incidence and poor prognosis, underscores the urgent need for enhanced treatment strategies (3). Despite the introduction of novel therapeutic approaches such as immunotherapy, chemoradiotherapy, and molecular therapy (5–7), the 5-year survival rate for advanced EC remains dismal (4). Unfortunately, these approaches have yielded unsatisfactory outcomes, particularly in regions with a high incidence of EC, such as China (8). Therefore, novel therapies targeting the oncogenesis of EC are urgently required.

Long non-coding RNAs (lncRNAs) have recently emerged as pivotal regulators in the initiation and progression of various tumors (9). These non-coding RNA transcripts, which exceed 200 nucleotides in length, regulate mRNA transcription and translation, protein stability, epigenetic modifications, and other critical biological processes (10, 11). FOXD2-AS1, previously associated with multiple tumor types, has also been implicated in the oncogenesis of EC. FOXD2-AS1, in collaboration with MACC1-AS1, mediates cisplatin resistance in ESCC cells through NSD2 induction (15). Overexpression of *FOXD2-AS1* is associated with cisplatin resistance in ESCC by targeting miR-195 and modulating the Akt/mTOR signaling pathway (16). Our previous research demonstrated that FOXD2-AS1 promotes proliferation and invasion through the miR-145-5p/CDK6 axis in EC (17). This study aims to elucidate the upstream mechanisms regulating the role of FOXD2-AS1 in EC.

N6-methyladenosine (m6A) RNA modification is the most prevalent RNA modification in eukaryotes and is regulated by three classes of enzymes: m6A methyltransferases (METTL3/14), m6A demethylases (ALKBH5 and FTO), and m6A reading enzymes (YTHDF1/2/3) (18). Recent studies have revealed the presence of m6A RNA modifications in various non-coding RNAs, including miRNAs, lncRNAs, and circRNAs (19). METTL3, an m6A methyltransferase, is an S-adenosylmethionine (SAM)-binding protein highly conserved across eukaryotes (20). The m6A methyltransferase complex plays a crucial role in RNA methylation modification. The core of this complex consists of a heterodimer composed of methyltransferase-like protein 3 (METTL3) and methyltransferase-like protein 14 (METTL14) (21). Among these components, METTL3 is the only catalytically active element, responsible for transferring methyl groups to the N6 position of adenine nucleotides in RNA. In contrast, METTL14 contributes to the structural stabilization of METTL3, facilitating

both the maintenance of the complex's integrity and the recognition of RNA substrates (22). YTH N6-methyladenosine RNA-binding protein 1 (YTHDF1) acts as a key reader enzyme of m6A RNA modifications (23), and there is increasing evidence supporting the role of m6A methylation in various cancers. In breast cancer, METTL3 has been shown to regulate MALAT1 expression, thereby modulating the E2F1/AGR2 axis and promoting resistance to adriamycin (24). YTHDF1 has also been implicated in driving breast cancer by enhancing FOXM1 translation in an m6A-dependent manner (25). However, the impact of m6A RNA modification on the initiation and progression of esophageal cancer (EC) through the regulation of lncRNA expression remains to be explored.

In this study, we first observed elevated METTL3 expression in esophageal cancer (EC) tissues and cells. Subsequently, loss-of-function experiments were performed to evaluate cell proliferation and apoptosis. Mechanistic investigations examined the molecular interplay between METTL3 and FOXD2-AS1, involving YTHDF1, in EC cells. Furthermore, *in vivo* experiments were conducted to assess the functional significance of the METTL3/FOXD2-AS1 axis in EC animal models.

EXPERIMENTAL

Bioinformatics prediction

The Encyclopedia of RNA Interactomes (ENCORI, https://starbase.sysu.edu.cn/index.php) (26) and The University of ALabama at Birmingham CANcer (UALCAN, https://ualcan.path.uab.edu/index.html) databases were used to analyze the expression of *METTL3* and *METTL14* in EC tissues and normal tissues (27–28). The sequence-based RNA adenosine methylation site predictor (SRAMP, http://www.cuilab.cn/sramp) (29–30) was used to analyze the m6A-modified sites in FOXD2-AS1. The correlation between *FOXD2-AS1* and *YTHDF1* in esophageal cancer was analyzed using the Gene Expression Profiling Interactive Analysis (GEPIA, http://gepia.cancer-pku.cn/)(31) database. All the above results were obtained on the TCGA-ESCA dataset (32).

Collection of clinical tissues

Clinical samples of esophageal cancerous and adjacent non-cancerous tissues were collected from 10 patients who underwent treatment at the Sixth Affiliated Hospital of Nantong University. The samples were immediately frozen in liquid nitrogen for preservation. None of the patients had received interventional therapy or systemic chemotherapy prior to surgery, and informed consent was obtained from either the patients or their legal guardians. All experiments were approved by the Ethics Committee of the Sixth Affiliated Hospital of Nantong University (2020-081).

Cell culture

Human normal esophageal epithelial cells (T-HEECs) and esophageal cancer (EC) cell lines (Eca-109 and /TE-1) were obtained from the Cell Resource Center of the Shanghai Academy of Sciences and cultured in DMEM supplemented with 10 % fetal

bovine serum (FBS) and 1 % penicillin-streptomycin. Cells were cultured in a humidified incubator at 37 °C with 5 % CO_2.

qRT-PCR analysis

Total RNA was isolated from tissues and cells using TRIzol reagent (Invitrogen, USA), followed by complementary DNA (cDNA) synthesis using the PrimeScript RT reagent kit (TaKaRa, Beijing). Quantitative PCR (qPCR) was performed using SYBR Green (Vazyme Biotech, Nanjing) on a GeneAmp 7500 system (Applied Biosystems, Thermo Fisher, USA). RNA expression levels were quantified using the $2^{-\Delta\Delta Ct}$ method (33), with GAPDH as the internal control. Primers were designed using the NCBI website (https://www.ncbi.nlm.nih.gov/tools/primer-blast/) (34). The amplification process was set as follows: the predenaturation stage lasted at 95 ℃ for 300 s, and then entered a cycling reaction. Each cycle included denaturation at 95 ℃ for 10 s and annealing at 60 ℃ for 30 s, a total of 45 cycles. The primer sequences used were as follows: METTL3, forward 5'-AAGCTGCACTTCAGACGAAT-3' and reverse 5'-GGAATCACCTCCGACACTC-3'; METTL14, forward 5'-GAACACAGAGCTTAAATCCCCA-3' and reverse 5'-TGTCAGCTAAACCTACATCCCTG-3'; FOXD2-AS1, forward 5'-TGGACCTAGCTGCAGCTCCA-3' and reverse 5'-AGTTGAAGGTGCACACACTG-3'; YTHDF1, forward 5'-ATGTCGGCCACCAGCGTGGACA-3' and reverse 5'-TCATTGTTTGTTTCGACTCTGC-3'; YTHDF2, forward 5'-CATGAATGGGAAGGGTCCCG-3' and reverse 5'-GACGAATGTGTCGCAGTTGG-3'; YTHDF3, forward 5'-TGTTGTGGACTATAATGCGTATGC-3' and reverse 5'-AAGCGAATATGCCGTAATTGGTTA-3'; GAPDH, forward 5'-GGAGCGAGATCCCTCCAAAAT-3' and reverse 5'-GGCTGTTGTCATACTTCTCATGG-3'.

Cell transfection

To silence the expression of FOXD2-AS1, siRNAs targeting FOXD2-AS1 (si*FOXD2-AS1*-1 and si*FOXD2-AS1*-2) were used. To reduce METTL3 expression, shMETTL3-1 and shMETTL3-2 were applied. As for the construction of shRNA expression vector, after designing synthetic primers based on *METTL3* gene transcript, the transformants were screened by colony PCR and verified by sequencing. For modulating YTHDF1 expression, si*YTHDF1* and pc-*YTHDF1* were employed. In control experiments, siNC or pc-DNA3.1 served as negative controls. These plasmid transfections from GenePharma were carried out in Eca-109 and TE-1 cells using Lipofectamine 2000 reagent (Invitrogen, USA). Sequences were as follows:

si*FOXD2-AS1-1*, sense: 5'-GGGCAAAGUUCGAGAGUGATT-3' and anti-sense: 5'-UCACUCUCGAACUUUGCCCTT-3'; si*FOXD2-AS1-2*, sense: 5'-GGACUGGUUCUGAGACAAATT-3'and anti-sense: 5'-UUUGU -CUCAGAACCAGUCCTT-3'(8); pc-DNA3.1: F-CTAGAGAACCCACTGCTTAC R-TAGAAGGCACAGTCGAGG. ShMETTL3-1 :

CcggGCCAAGGAACAATCCATTGTTCTCGAGAACAATGGATTGTTCCTTGGC TTTTTTg; shMETTL*3*-2: CcggCGTCAGTATCTTGGGCAAGTTCTCGAGAACTTGCCCAAGATACTGACG TTTTTTg; shNC: CcggGCTGCACTTCAGACGAATTATCTCGAGATAATTCGTCTGAAGTGCAGC TTTTTTg.

Cell counting kit 8 (CCK-8) assay

$1*10^4$ cells were seeded into each well of a 96-well plate. Subsequently, 10 μL of CCK-8 (Dojindo, Shanghai) reagent was introduced into each well, and cells were cultured using serum-free medium (12309019, Thermo, USA). This process was carried out at 24, 48, and 72 hours. After a 2-hour incubation, the absorbance at 450 nm in each well was measured using a microplate reader (BioTex, USA).

EdU incorporation assay

Cells were incubated with 10 mM EdU for 2 h, then fixed with 4 % paraformaldehyde, permeabilized with 0.3 % Triton X-100, and stained with Apollo fluorescent dye (Sigma-Aldrich, Shanghai). Nuclei were stained with 5 mg/mL 4 ', 6-diamidino-2-phenylindole (DAPI) (D9542, Sigma, Shanghai) for 10 minutes. The number of EdU-positive cells in five random fields was counted under the Zeiss UV LSM 510 confocal microscope. All experimental procedures were performed according to the instructions of the kit (C0078S, Beyotime, China).

Flow cytometry

To assess the apoptosis ability of tumor cells, the PE Annexin V Apoptosis Detection Kit I (BD Pharmingen) was employed. Cells were harvested, resuspended in 1 × binding buffer, and collected in a 10 ml centrifuge tube. Incubation with 5-μL PE Annexin V and 5-μL 7-AAD was conducted for 15 min. Apoptotic cells were assessed using a FACS Calibur flow cytometer (BD Bioscience, USA).

Western blotting

To assess the protein expression of METTL3, METTL14, YTHDF1, Bax, c-caspase-3, t-caspase-3, PCNA, and Ki-67 in Esophageal cancer cells and tissues, protein extraction was performed using RIPA lysis buffer (Beyotime). The protein concentration was determined using a BCA Protein assay kit (Beyotime). Subsequently, the proteins were separated on SDS-PAGE and transferred onto PVDF membranes. Blocking was achieved using 5 % skimmed milk (P0216, Beyotime). Primary antibodies against METTL3(1:1000; 67733-1-IG, Proteintech, China) METTL14 (1:1000; F1391, Selleck, Shanghai) YTHDF1(1:500; 66745-1-IG, Proteintech, Wuhan), Bax(1:1000; Cat. #2772T, CST, Shanghai), c-caspase-3(1:1000; Cat. #9661T, CST, Shanghai), t-caspase-3(1:1000; 82202-1-RR, Proteintech), PCNA(1:500; Cat. #13110T, CST, Shanghai), Ki-67 (1:700; ab15580, Abcam, Shanghai), and GAPDH (1：1000； sc-32233, Santa Cruz Biotechnology, USA) were incubated overnight using a 5 % milk dilution followed by incubation with HRP-labeled goat anti-rabbit IgG. The blots were

then visualized using chemiluminescence (HRP Substrate) and captured with an AlphaView analysis system (ProteinSimple) (FluorChem R, USA). GAPDH was used as a referent protein for calculating protein expression, protein band quantification was performed using ImageJ software (.v1.8.0) (35).

Quantification of m6A RNA methylation

Total RNA was extracted from cells following the manufacturer's instructions, using TRIzol reagent (Thermo Fisher, USA). m6A RNA methylation levels were quantified using the EpiQuik m6A RNA Methylation Quantification Kit (Colorimetric; Epigentek) and measured at an absorbance of 450 nm.

RNA stability assays

Cells were seeded in 6-well plates and transfected with either shNC or shMETTL3. Following transfection, cells were treated with actinomycin D (CST, 5 μg/ml, Shanghai) for 0, 4, and 8 hours. RNA was then extracted to evaluate the levels of the target RNA via real-time PCR.

Co-IP

To investigate the interaction between METTL3 and YTHDF1 proteins, we performed a Co-IP (co-immunoprecipitation) assay. We first constructed the METTL3-Myc© expression vector by fusing the METTL3 coding sequence with the pc-AMBIA1300-35S-Myc-rbcsE9 vector (NM_019852.5). (F-CGCAAATGGGCGGTAGGCGTG; R-CATAGCGTAAAAGGAGCAACA). Similarly, we generated the YTHDF1-GFP© expression vector by amplifying and fusing the coding sequence of YTHDF1 with the pC-AMBIA1300-35S-GFP-rbcsE9 vector (NM_017798.4) (F- CGCAAATGGGCGGTAGGCGTG; R-GACACGCTGAACTTGTGGC). Subsequently, these expression vectors were transfected into the appropriate cells. The cells were lysed under non-denaturing conditions, and the resulting lysate was collected. The lysate was then incubated with either anti-GFP (P2132, Beyotime, Shanghai) or anti-MYC (P2118, Beyotime, Shanghai) beads at 4 °C for 4 hours. Following incubation, we carried out five washes using an extraction buffer. Subsequently, we eluted the proteins from the magnetic beads by boiling the samples in the SDS sample buffer for 10 minutes. Afterward, we isolated the proteins via SDS-PAGE electrophoresis and performed Western Blots to detect the presence of the proteins.

RNA immunoprecipitation (RIP)

To validate the interaction between *FOXD2-AS1* and *YTHDF1*, *YTHDF2*, or *YTHDF3*, we performed RNA immunoprecipitation (RIP) using the EZMagna RIP Kit (Millipore, USA). After washing and scraping the cells with PBS, they were centrifuged and resuspended in complete RIP lysis buffer. Antibodies (IgG, YTHDF1, YTHDF2, and YTHDF3) were pre-incubated with Protein A/G magnetic beads in an immunoprecipitation buffer. The cell lysates were then incubated with the antibody-bead complexes overnight at 4 °C. The RNA eluted from the beads was precipitated

with ethanol, dissolved in RNase-free water, and analyzed by qPCR to assess FOXD2-AS1 expression. The antibodies used were IgG (10284-1-AP, Proteintech, Wuhan), YTHDF1 (#86463, CST, Shanghai), YTHDF2 (24744-1-AP, Proteintech), and YTHDF3 (#24206S, CST, Shanghai).

M6A MeRIP qPCR

To quantify the m6A methylation level of FOXD2-AS1, we performed m6A methylated RNA immunoprecipitation (MeRIP) using an m6A-specific antibody and the Magna m6A MeRIP Kit (Millipore, USA). Following cell treatment (transfection with shNC, shMETTL3-1, and shMETTL3-2), RNA was extracted from Eca-109 and TE-1 cells using the Trizol reagent (Invitrogen, USA). After fragmenting the RNA, immunoprecipitation was carried out using m6A or IgG antibodies in 1 ml of buffer supplemented with ribonuclease inhibitors. Following washing, protein A/G magnetic beads were added to the mixture and incubated for 2 hours at 4 °C. The m6A RNA was then eluted using N6-methyladenosine-5'-monophosphate sodium salt at 4 °C for 1 hour, followed by RNA purification and qPCR analysis to investigate the regulation of *FOXD2-AS1* by *METTL3*.

RNA pull-down assay

To investigate the binding interaction between *YTHDF1* and *FOXD2-AS1*, we performed an RNA pull-down assay. A biotinylated FOXD2-AS1 probe was designed and synthesized by RiboBio. The cells were transfected with the probe and treated for 2 days. Subsequently, the cells were washed, lysed, and incubated at 4 °C with Dynabeads™ M-280 Streptavidin magnetic beads (Invitrogen, USA). The precipitated proteins were then purified using TRIzol for western blot analysis.

Animal models

The procedures involving animal assays were conducted following approval from the Ethical Committee of Affiliated Hospital 6 of Nantong University (XMLL-2021-808). A total of 24 BALB/c nude mice, aged 4-6 weeks and weighing 18-20 grams, were subcutaneously injected with cells transfected with various constructs, including a blank vector (NC group), shMETTL3-1 (METTL3 KD group), pc-FOXD2-AS1 (FOXD2-AS1 OE group), and shMETTL3-1+pc-FOXD2-AS1 (METTL3 KD+FOXD2-AS1 OE group). The injections were administered to the right flank of the mice. Over a 28-day period, tumor volume measurements were taken every 3 days, and the recorded data were calculated using the formula (length×width2)/2. Additionally, upon sacrificing the mice, the tumors were excised, and their weights were measured.

FISH

Specific FISH probes for *FOXD2-AS1* were designed and synthesized by Servicebio (Wuhan, China). Hybridization was performed in mouse tumor tissue, as previously reported (36). All images were analyzed using a fluorescence microscope. The FISH probe sequence for *FOXD2-AS1* was as follows: 5'-TAAAATTAGAGAAATCTGCGGGCGTAGTTCCCCAAGC-3'.

Immunohistochemistry (IHC)

Formalin-fixed tissue samples were sectioned into 5-μm slices. Subsequently, dewaxing, hydration, and heat-induced epitope retrieval were performed. The sections were treated with a primary antibody against METTL3 (1:1000; 67733-1-IG, Proteintech)，Ki-67 (1:1000; ab15580, Abcam, Shanghai) followed by incubation with secondary antibodies (1:3000; ab205719, Abcam, Shanghai) and peroxidase-conjugated streptavidin. A 3,3'-diaminobenzidine tetrahydrochloride (DAB) solution (36201ES03, Yeasen. Shanghai) was applied for 5 minutes, and counterstaining was carried out with hematoxylin. The stained sections were then observed under a light microscope. For protein quantification of METTL3: the number of METTL3-positive cells in five random areas was counted at 40 × magnification, and the average value was the number of METTL3-positive cells in that section.

Hematoxylin and eosin (HE) staining

Paraffin-embedded tissue sections were subjected to a 30 min roasting process (70 ℃), followed by dewaxing and hydration. The cell nuclei were stained with hematoxylin solution (Biosharp, Beijing), and the cytoplasm was stained with eosin solution (Biosharp). After the sections were allowed to dry, they were preserved using a neutral resin.

Statistical analysis

All experiments were performed in triplicate, statistical significance was determined at a level of $p < 0.05$. Statistical analyses were conducted using SPSS 21.0 software (IBM). Differences were assessed using either the student’s t-test or one-way ANOVA (Tukey's post hoc test). Additionally, a ROC curve was generated to assess the diagnostic value of FOXD2-AS1 expression for EC patients.

RESULTS AND DISCUSSION

METTL3 was upregulated in EC tissues and cells

ENCORI database analysis revealed a significant increase in *METTL3* expression in EC tissues compared to normal tissues, with no significant change in *METTL14* expression (Fig. 1a). Furthermore, UALCAN database analysis showed that *METTL3* expression increased with tumor grade, while *METTL14* expression remained relatively unchanged (Fig. 1c). The receiver operating characteristic (ROC) curve showed that the expression level of *METTL3* in esophageal cancer had potential diagnostic value (Fig. 1b) (32). The expression of METTL3 protein in tissues was confirmed through WB, revealing a significant upregulation of METTL3 in cancerous tissues compared to normal tissues (Fig. 1D) ($p < 0.001$). To validate these predictions, METTL3 and METTL14 mRNA levels were assessed in tissues and cells using qRT-PCR. In comparison to normal tissues, only METTL3 showed a significant upregulation in cancerous tissues (Fig. 1E) ($p < 0.001$). High levels of METTL3 were observed in Eca-

109 and TE-1 cells compared to HEEC (Fig. 1F) ($p < 0.001$, $p = 0.023$). In summary, *METTL3* is significantly overexpressed in EC tissues and cells.

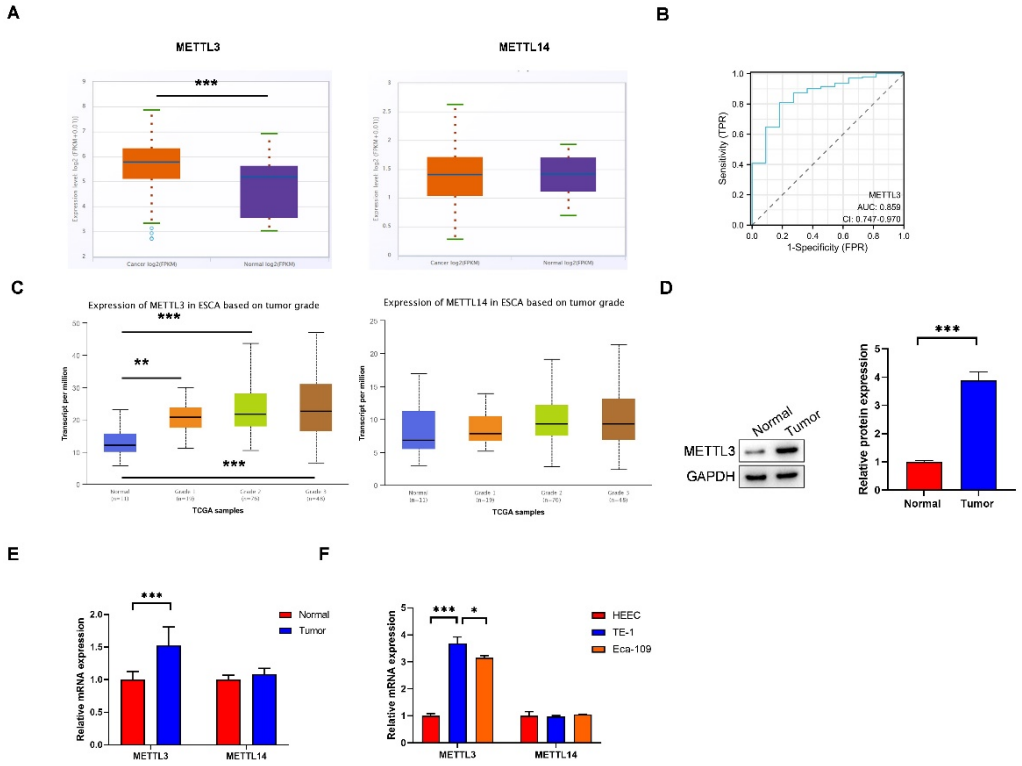

Fig. 1. METTL3 expression was upregulated in EC tissues and cells: a) ENCORI analysis of elevated *METTL3* expression and unaltered *METTL14* expression in EC tissues compared to normal tissues; b) ROC curve analysis evaluating the potential diagnostic value of *METTL3* expression levels in esophageal cancer; c) UALCAN database analysis of *METTL3* and *METTL14* expression based on tumor grade; d) WB analysis of METTL3 expression in the samples; e) qRT-PCR analysis showing the expression levels of *METTL3* and *METTL14* in 10 matched EC and non-tumor tissues; f) qRT-PCR analysis of *METTL3* and *METTL14* expression in HEEC, Eca-109, and TE-1 cells. $^{*}p < 0.05$, $^{**}p < 0.01$, $^{***}p < 0.001$.

METTL3 silencing suppressed proliferation and accelerated apoptosis of EC cells

To investigate the functional role of METTL3 in EC, qRT-PCR results confirmed the successful silencing of *METTL3* (Fig. 2a) (ECA-109: shNC *vs.* shMETTL3-1, $p < 0.001$; shNC *vs.* shMETTL3-2, $p < 0.001$) (TE-1: shNC *vs.* shMETTL3-1, $p < 0.001$; shNC *vs.* shMETTL3-2, $p < 0.001$). Following *METTL3* knockdown, the total m6A level was also reduced (Fig. 2b) (ECA-109: shNC *vs.* shMETTL3-1, $p < 0.001$; shNC *vs.* shMETTL3-2, $p < 0.001$) (TE-1: shNC *vs.* shMETTL3-1, $p < 0.001$; shNC *vs.* shMETTL3-2, $p < 0.001$). The CCK-8 assay demonstrated that *METTL3* downregulation inhibited cell proliferation (Fig. 2C) (ECA-109: shNC *vs.* sh *METTL3*-1, $p < 0.001$; shNC *vs.* shMETTL3-2, $p < 0.001$) (TE-1: shNC *vs.* shMETTL3-1, $p < 0.001$; shNC *vs.* shMETTL3-2, $p < 0.001$). The EdU assay showed a decrease in the abundance of proliferating cells when *METTL3* expression was downregulated (Fig.

2d,g) (ECA-109: shNC *vs.* shMETTL3-1, $p < 0.001$; shNC *vs.* shMETTL3-2, $p < 0.001$) (TE-1: shNC *vs.* shMETTL3-1, $p < 0.001$; shNC *vs.* shMETTL3-2, $p < 0.001$). Flow cytometry analysis revealed an increase in apoptotic cells following *METTL3* knockdown (Fig. 2e,h) (Eca-109: shNC *vs.* shMETTL3-1, $p = 0.009$; shNC *vs.* sh *METTL3*-2, $p = 0.008$) (TE-1: shNC *vs.* shMETTL3-1, $p = 0.007$; shNC *vs.* sh METTL3-2, $p = 0.008$). WB analysis showed that the expression levels of the proapoptotic proteins Bax and c-caspase-3 increased after *METTL3* knockdown, while there was no significant change in t-caspase-3 levels. Additionally, the levels of proliferation-related proteins Ki-67 and PCNA decreased compared to the control group (Fig. 2F) (BAX: shNC *vs.* shMETTL3-1, $p < 0.001$; shNC *vs.* shMETTL3-2, $p < 0.001$) (c-caspase-3: shNC *vs.* shMETTL3-1, $p < 0.001$; shNC *vs.* shMETTL3-2, $p < 0.001$) (Ki-67: shNC *vs.* shMETTL3-1, $p < 0.001$; shNC *vs.* shMETTL3-2, $p < 0.001$) (PCNA: shNC *vs.* shMETTL3-1, $p < 0.001$; shNC *vs.* shMETTL3-2, $p < 0.001$). These findings illustrate that METTL3 inhibition impedes proliferation，while inducing apoptosis in EC.

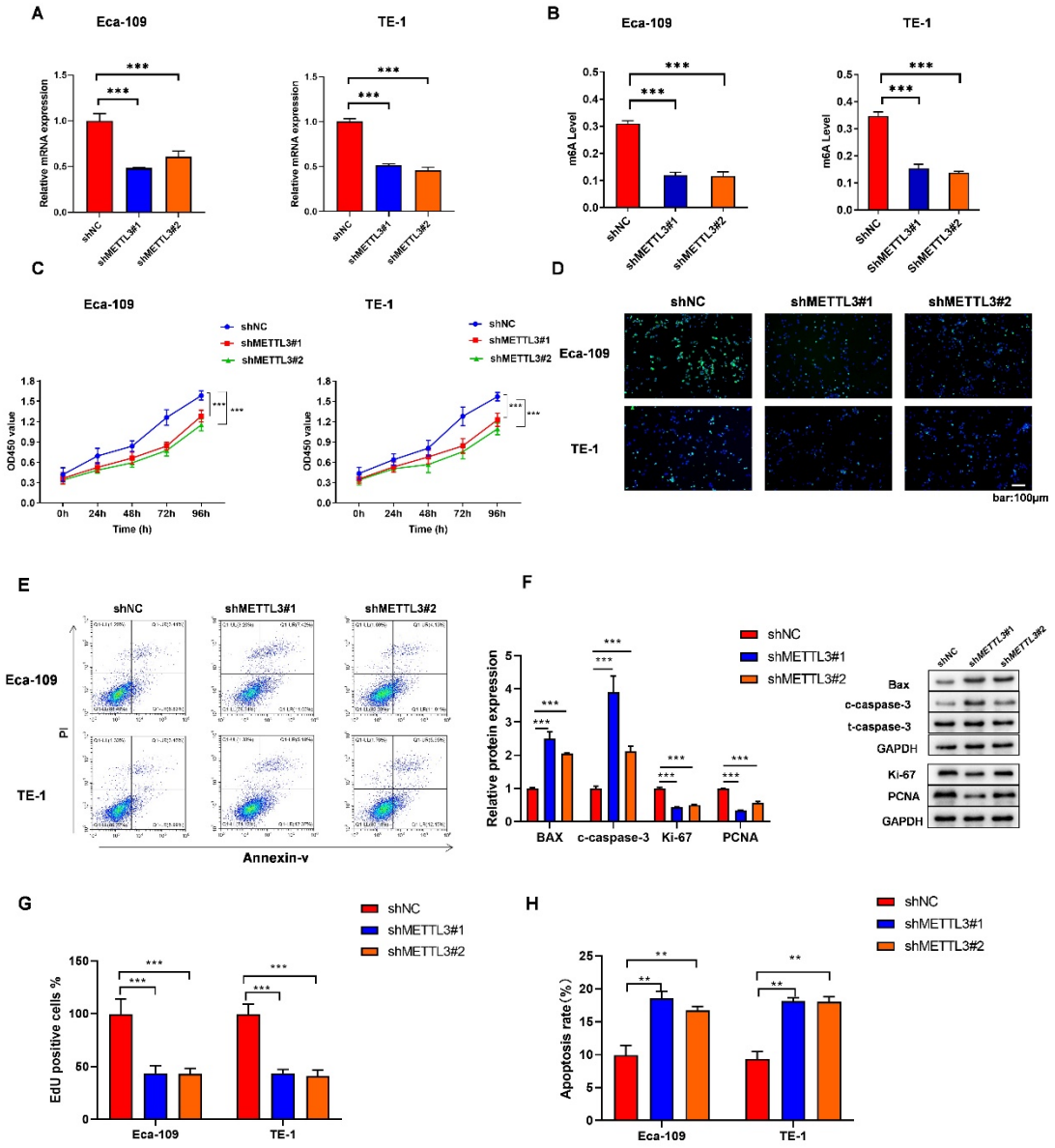

Fig. 2. METTL3 silencing suppressed proliferation and accelerated apoptosis of EC cells: a) mRNA expression of METTL3 in Eca-109 and TE-1 cells treated with shNC, shMETTL3-1, and shMETTL3-2 to confirm transfection efficiency by qRT-PCR; b) m6A RNA methylation was estimated using a colorimetric method; c) cell proliferation of transfected Eca-109 and TE-1 cells assessed by performing a CCK-8 experiment; d) EdU incorporation assay in Eca-109 and TE-1 cells; e) Apoptosis of Eca-109 and TE-1 cells was tested by flow cytometry. (F) Bax, c-caspase-3, t-caspase-3, Ki67, and PCNA proteins are expressed in Eca-109 cells with or without shMETTL3; g) and h) quantified data of EdU incorporation assay and flow cytometry. *$p < 0.05$, **$p < 0.01$, ***$p < 0.001$.

METTL3 regulated the m6A modification of FOXD2-AS1

SRAMP predicted 12 m6A-modified sites (Fig. 3a). Several of the analyze binding sites showed above moderate confidence. MeRIP assays revealed that the m6A level in Eca-109 and TE-1 cells was higher than that in HEEC cells (Fig. 3b) (HEEC: Input *vs.* IgG, $p < 0.001$; Input *vs.* m6A, $p < 0.001$) (Eca-109: Input *vs.* IgG, $p < 0.001$; Input *vs.* m6A, $p = 0.007$) (TE-1: Input *vs.* IgG, $p < 0.001$; Input *vs.* m6A, $p = 0.006$) (m6A content: HEEC cells *vs.* TE-1 cells, $p = 0.006$; HEEC cells *vs.* Eca-109 cells, $p = 0.017$). During qRT-PCR experiments, *FOXD2-AS1* expression was significantly reduced upon METTL3 inhibition (Fig. 3C) (Eca-109: shNC *vs.* shMETTL3-1, $p < 0.001$; shNC *vs.* shMETTL3-2, $p < 0.001$) (TE-1: shNC *vs.* shMETTL3-1, $p < 0.001$; shNC *vs.* shMETTL3-2, $p < 0.001$). Subsequently, the effect of *METTL3* knockdown on the stability of FOXD2-AS1 was investigated, revealing that *METTL3* knockdown improved the stability of *FOXD2-AS1* RNA in Eca-109 and TE-1 cells (Fig. 3D) (Eca-109:4h- shNC *vs.* shMETTL3-1, $p < 0.001$; shNC *vs.* shMETTL3-2, $p = 0.0002$; 8h-shNC *vs.* shMETTL3-1, $p < 0.001$; shNC *vs.* shMETTL3-2, $p = 0.010$) (TE-1: 4h- shNC *vs.* shMETTL3-1, $p < 0.001$; shNC *vs.* shMETTL3-2, $p = 0.023$; 8h- shNC *vs.* shMETTL3-1, $p = 0.008$; shNC *vs.* shMETTL3-2, $p = 0.004$). Moreover, *METTL3* silencing decreased the m6A level in Eca-109 and TE-1 cells (Fig. 3E) (Eca-109:sh-NC- Input *vs.* IgG, $p < 0.001$; Input *vs.* m6A, $p = 0.043$; shMETTL3-1- Input *vs.* IgG, $p < 0.001$; Input *vs.* m6A, $p = 0.009$; sh*METTL3*-2- Input *vs.* IgG, $p < 0.001$; Input *vs.* m6A, $p = 0.008$) (TE-1: shNC- Input *vs.* IgG, $p < 0.001$; Input *vs.* m6A, $p = 0.007$; shMETTL3-1- Input *vs.* IgG, $p < 0.001$; Input *vs.* m6A, $p = 0.0004$; shMETTL3-2-Input *vs.* IgG, $p < 0.001$; Input *vs.* m6A, $p < 0.001$). These results clarify that METTL3 modulates the m6A modification of FOXD2-AS1 in EC.

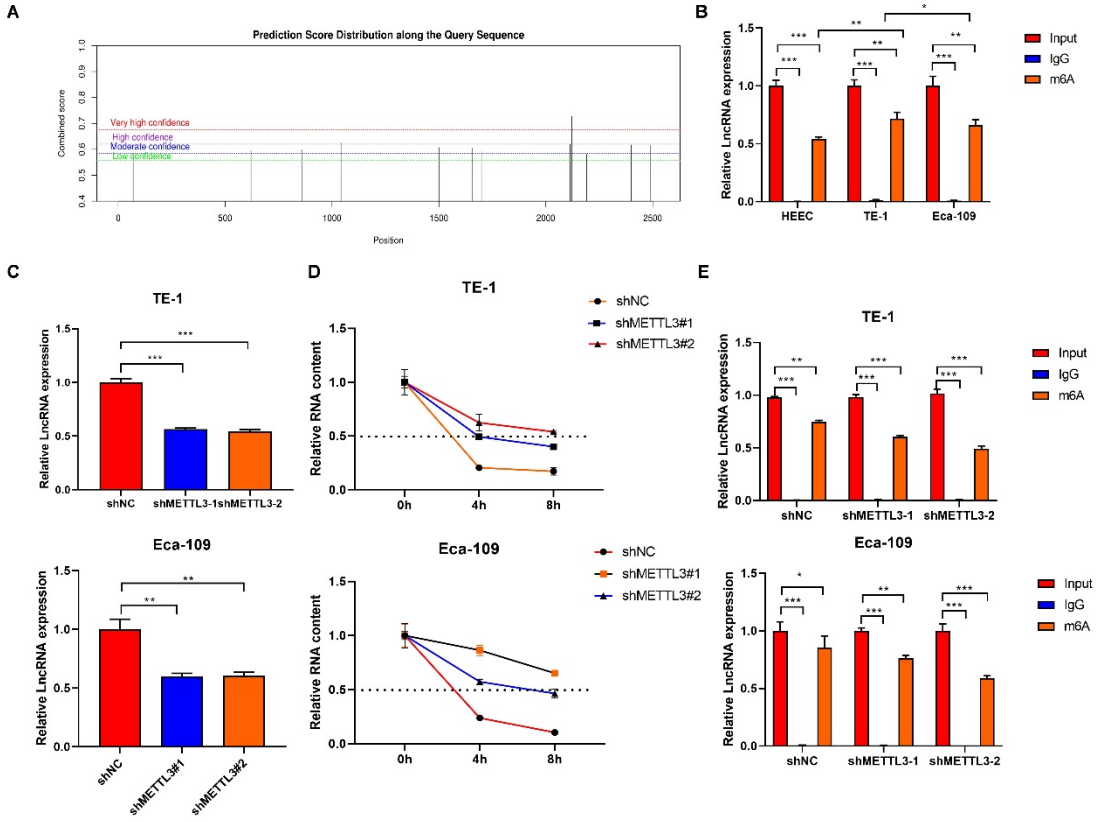

Fig. 3 METTL3 regulated the m6A modification of FOXD2-AS1.

(A) Analysis of m6A-modified sites in FOXD2-AS1 by SRAMP. (B) MeRIP-qPCR analysis of m6A levels in HEEC, TE-1 and Eca-109 cells. (C) qRT-PCR results showing the expression of FOXD2-AS1 after transfection with siNC, shMETTL3-1, and shMETTL3-2. (D) Evaluation of FOXD2-AS1 RNA stability in TE-1 and Eca-109 cells with or without *METTL3* shRNA. (E) MeRIP-qPCR analysis of m6A levels following *METTL3* silencing in TE-1 and Eca-109 cells. $^{*}p < 0.05$, $^{**}p < 0.01$, $^{***}p < 0.001$.

YTHDF1 bound with FOXD2-AS1

To identify the functional proteins involved in the m6A modification of FOXD2-AS1, RIP experiments were conducted. YTHDF1, YTHDF2, and YTHDF3 were found to bind with FOXD2-AS1, with YTHDF1 exhibiting the highest affinity (Fig. 4A-C) (Eca-109: IgG *vs.* YTHDF1, $p < 0.001$; TE-1-IgG *vs. YTHDF1*, $p < 0.001$) (Eca-109: IgG *vs.* YTHDF2, $p < 0.001$; TE-1-IgG *vs.* YTHDF1, $p < 0.001$) (ECA-109: IgG *vs.* YTHDF3, $p < 0.001$; TE-1-IgG *vs.* YTHDF3, $p < 0.001$). The positive correlation between *YTHDF1* and *FOXD2-AS1* in EC was analyzed by GEPIA (Pearson correlation coefficient) (R = 0.38, $p < 0.001$) (Fig. 4D). RNA pull-down experiments validated the interaction between the YTHDF1 protein and FOXD2-AS1 (Fig. 4E). Subsequently, YTHDF1 was either upregulated or downregulated, and the transfection efficacy was confirmed by western blot (Fig. 4F-G) (Fig.4 F: Eca-109: shNC *vs.* shMETTL3-1, $p < 0.001$; TE-1: shNC *vs.* shMETTL3-1, $p < 0.001$) (Fig.4 G: Eca-109: Vector *vs. YTHDF1*, $p = 0.006$; TE-1: Vector *vs. YTHDF1*, $p = 0.005$) *FOXD2-AS1* expression was

significantly increased or decreased after *YTHDF1* overexpression or knockdown, as assessed by qRT-PCR (Fig. 4H) (Eca-109: shNC *vs.* shYTHDF1, $p < 0.001$; Vector *vs.* *YTHDF1*, $p = 0.005$;TE-1: shNC *vs.* shYTHDF1, $p < 0.001$; Vector *vs.* *YTHDF1*, $p < 0.001$). Co-IP experiments confirmed the interaction between METTL3 protein and YTHDF1 protein (Fig. 4I). Moreover, RIP experiments confirmed that the interaction between *YTHDF1* and *FOXD2-AS1* was modulated when *METTL3* expression was downregulated or upregulated (Fig. 4J) (Left: Eca-109: IgG: Vector *vs.* *METTL3*, $p = 0.767$;*YTHDF1*: Vector *vs.* *METTL3*, $p = 0.006$; TE-1: IgG: Vector *vs.* *METTL3*, $p = 0.835$;*YTHDF1*: Vector *vs.* *METTL3*, $p = 0.004$) (Right: Eca-109: IgG: shNC *vs.* shMETTL3, $p = 0.713$;*YTHDF1*: shNC *vs.* shMETTL3, $p < 0.001$; TE-1: IgG: shNC *vs.* shMETTL3, $p = 0.849$;*YTHDF1*: shNC *vs.* shMETTL3, $p = 0.037$). These results collectively demonstrate that METTL3 regulates the interaction between YTHDF1 and FOXD2-AS1.

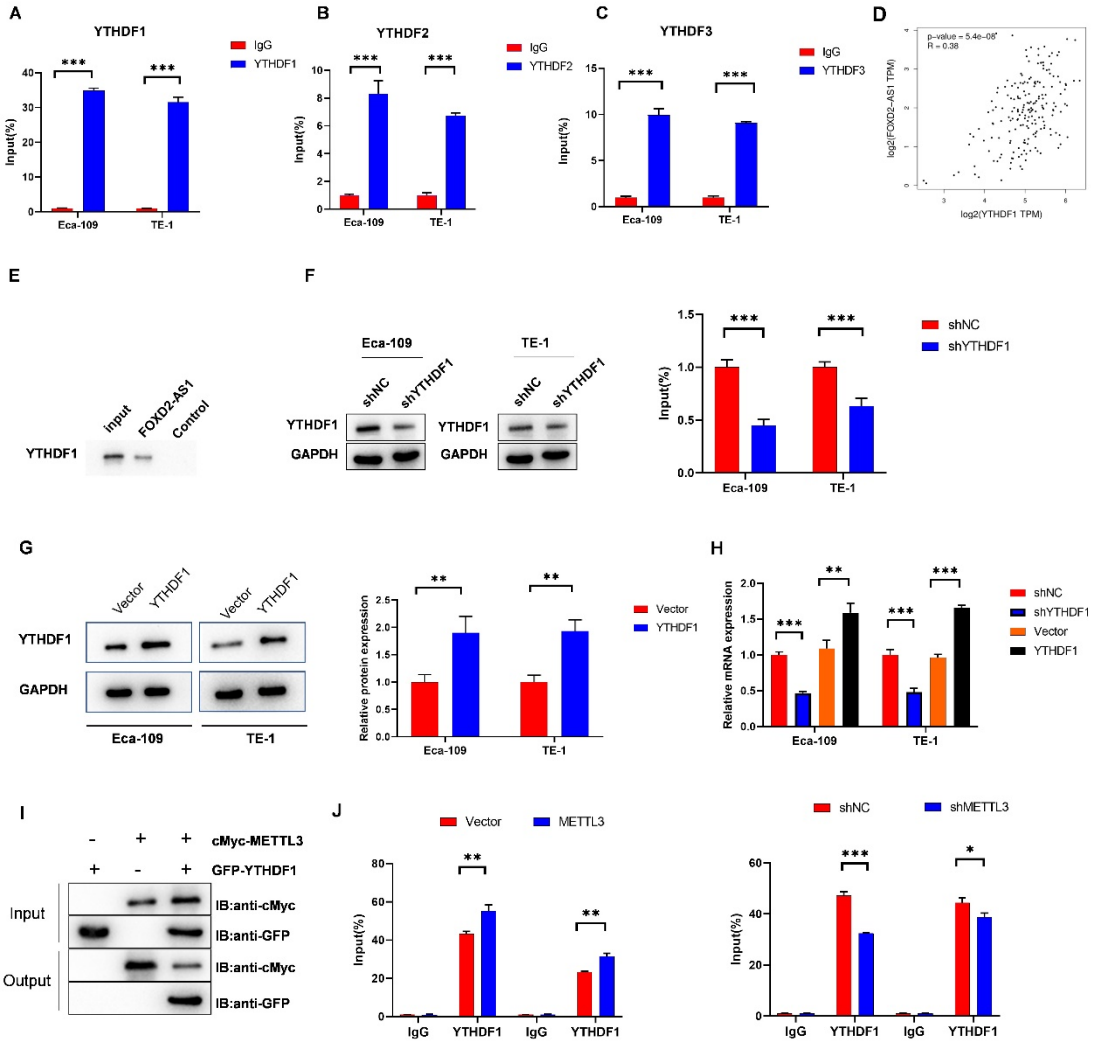

Fig. 4. YTHDF1 interaction with FOXD2-AS1: a) to c) RIP assay measured the binding affinity of FOXD2-AS1 with m6A methylation-reading proteins YTHDF1, YTHDF2, and YTHDF3; d) GEPIA analyzed a positive correlation between FOXD2-AS1 and YTHDF1 in EC; e) RNA pull-down analysis determined the binding of FOXD2-AS1 with YTHDF1; f) to h) Tumor cells were transfected with shNC, shYTHDF1, vector,

and YTHDF1, and their effects were assessed by western blot. Changes in *FOXD2-AS1* expression following YTHDF1 downregulation or upregulation were explored using qRT-PCR. (I) CO-IP assay probed the interaction between METTL3 and YTHDF1. (J) RIP assay investigated the effects of *METTL3* knockdown or upregulation on the interaction between FOXD2-AS1 and YTHDF1. The impact of METTL3 depletion on their binding was also estimated through RIP assay. $^{*}p < 0.05$, $^{**}p < 0.01$, $^{***}p < 0.001$.

METTL3 regulated FOXD2-AS1 m6A modification to affect EC *in vivo*

Animal models were categorized into the NC group, METTL3 KD group, FOXD2-AS1 OE group, and METTL3 KD+FOXD2-AS1 OE group. Tumor sizes and volumes were significantly smaller in the METTL3 KD group than in the NC group, while larger tumor sizes and volumes were observed in the FOXD2-AS1 OE group. Tumor sizes and volumes were significantly larger in the FOXD2-AS1 OE group compared to the METTL3 KD group (Fig. 5a,b) (Fig. 5b: NC *vs.* METTL3 KD, $p < 0.001$； NC *vs.* FOXD2-AS1 OE, $p < 0.001$; *METTL3* KD *vs.* METTL3 KD+FOXD2-AS1 OE, $p = 0.004$; METTL3 KD+FOXD2-AS1 OE *vs.* FOXD2-AS1 OE, $p < 0.001$) (Fig. 5c: NC *vs.* METTL3 KD, $p < 0.001$；NC *vs.* FOXD2-AS1 OE, $p = 0.048$; METTL3 KD *vs.* METTL3 KD+FOXD2-AS1 OE, $p = 0.005$; METTL3 KD+FOXD2-AS1 OE *vs.* FOXD2-AS1 OE, $p = 0.049$). Additionally, tumor weights were significantly reduced with METTL3 silencing but markedly increased with *FOXD2-AS1* overexpression. Furthermore, tumor weights in the METTL3 KD+FOXD2-AS1 OE group were significantly heavier compared to the METTL3 KD group (Fig. 5c)(NC *vs.* METTL3 KD, $p = 0.005$； NC *vs.* FOXD2-AS1 OE, $p = 0.527$; METTL3 KD *vs.* METTL3 KD+FOXD2-AS1 OE, $p = 0.298$; METTL3 KD+FOXD2-AS1 OE *vs.* FOXD2-AS1 OE, $p = 0.005$). qRT-PCR analysis of tissues indicated that FOXD2-AS1 expression was decreased after *METTL3* knockdown but enhanced following *FOXD2-AS1* overexpression vector transfection. Moreover, the decrease in FOXD2-AS1 due to *METTL3* silencing was reversed by FOXD2-AS1 overexpression vector transfection (Fig. 5D-E) (NC *vs.* METTL3 KD, $p < 0.001$； NC *vs.* FOXD2-AS1 OE, $p = 0.005$; METTL3 KD *vs.* METTL3 KD+FOXD2-AS1 OE, $p = 0.007$; METTL3 KD+FOXD2-AS1 OE *vs.* FOXD2-AS1 OE, $p = 0.006$). Upregulation of FOXD2-AS1 abrogated the mitigation of tissue injury caused by *METTL3* silencing. FISH experiments revealed FOXD2-AS1 expression in tumor tissue, confirming that *FOXD2-AS1* expression was reduced after *METTL3* knockdown but enhanced after *FOXD2-AS1* overexpression vector transfection. Immunohistochemistry revealed the expression levels of METTL3 and Ki67 in tumor tissues, with *METTL3* knockdown reversing the upregulation of Ki67 levels caused by *FOXD2-AS1* overexpression. However, *METTL3* expression in the METTL3 KD group was downregulated, while *METTL3* expression in other groups remained unchanged (Fig. 5f). Thus, METTL3 mediated FOXD2-AS1 m6A modification to affect EC *in vivo*.

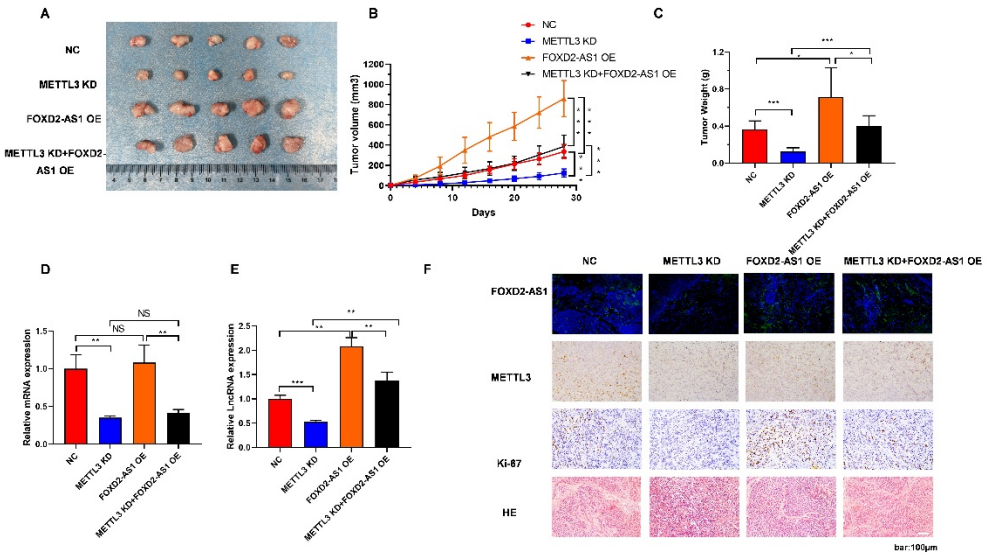

Fig. 5. METTL3 regulated FOXD2-AS1 m6A modification to affect EC *in vivo*. Animals were divided into NC group, METTL3 KD group, FOXD2-AS1 OE group and METTL3 KD+FOXD2-AS1 OE group. a) pictures of tumors were exhibited; b) tumor volumes were measured every third day; c) tumor weights were recorded and plotted as histogram; d) qRT-PCR analysis of the METTL3 expression in tissues of four groups; e) qRT-PCR analysis of the FOXD2-AS1 expression in tissues of four groups; f) Representative images of FISH staining for FOXD2-AS1, immunohistochemical staining for METTL3 and Ki-67, and HE staining of the tumors of mice. $^{*}p < 0.05$, $^{**}p < 0.01$, $^{***}p < 0.001$.

FOXD2-AS1, recognized for its role as an oncogene in esophageal cancer (EC), has been implicated in several aspects of the disease. For instance, Xue et al. demonstrated that FOXD2-AS1, in collaboration with MACC1-AS1, mediates cisplatin resistance in ESCC cells through NSD2 (15). Liu et al. revealed that *FOXD2-AS1* overexpression induces cisplatin resistance in ESCC by interacting with miR-195 to regulate the Akt/mTOR pathway (16). Additionally, our previous work has demonstrated that FOXD2-AS1 enhances the proliferation and invasion capacities of EC cells via the miR-145-5p/CDK6 axis (17). Based on these findings, we systematically explored the mechanisms regulating *FOXD2-AS1* in EC.

Extensive research has revealed the critical involvement of dysregulated m6A RNA methylation in various cancers, where it can exert either enhancing or suppressive effects (37, 38). Furthermore, emerging evidence suggests that long non-coding RNAs play a role in modulating METTL3 in various carcinomas. For example, in non-small-cell lung cancer, METTL3 promotes ABHD11-AS1 expression to enhance the Warburg effect (39). METTL3 has also been shown to stabilize the lncRNA SNHG7, thereby regulating the SRSF1/c-Myc axis and accelerating glycolysis in prostate cancer (40). Notably, we identified 12 m6A-mediated sites on *FOXD2-AS1* using SRAMP, suggesting METTL3's involvement in the regulation of *FOXD2-AS1*. Moreover, predictions from the ENCORI database indicate that only *METTL3*, not *METTL14*, exhibits relatively high expression in EC. Consistently, we observed upregulation of

METTL3 expression in EC tissues and cells compared to normal counterparts. Subsequent functional experiments revealed that inhibition of METTL3 impedes proliferation and induces apoptosis in Eca-109 and TE-1 cells. These results suggest that *METTL3* may regulate EC proliferation and apoptosis. Additionally, MeRIP assays confirmed a high m6A level on FOXD2-AS1, which was decreased when *METTL3* expression was silenced, suggesting that FOXD2-AS1 might be mediated by METTL3 in an m6A-dependent manner.

Previous research has highlighted the crucial roles of m6A readers in facilitating the processing of m6A RNA methylation. For example, Anita et al. found that the dysregulation of m6A readers YTHDF1 and YTHDF3 is associated with metastasis and prognosis in breast cancer patients (41). In liver cancer, YTHDF2 was shown to facilitate the stem cell phenotype and metastasis by influencing OCT4 levels (42) . To uncover the m6A reader involved in the modulation of FOXD2-AS1 by METTL3, we conducted RIP assays to measure the binding affinity between YTHDF1, YTHDF2, or YTHDF3 with FOXD2-AS1. Our results revealed the highest binding affinity between YTHDF1 and FOXD2-AS1, and this positive correlation was further supported by predictions from the GEPIA database. Subsequent mechanistic assays confirmed that METTL3 could influence the binding of YTHDF1 to FOXD2-AS1. Moreover, in *in vivo* assays, we demonstrated that METTL3 regulates FOXD2-AS1 to control EC tumor growth. This study represents the first exploration of m6A RNA methylation in EC and the mechanism underlying the METTL3/YTHDF1/FOXD2-AS1 axis in EC.

CONCLUSIONS

Our findings suggest that METTL3 regulates FOXD2-AS1 in an m6A-dependent manner through its interaction with YTHDF1, ultimately mediating the proliferation and apoptosis abilities of EC cells. These discoveries provide valuable insights into potential therapeutic targets for the treatment of EC patients.

Conffficts of interest. – The authors declare no conffict of interest.

Funding. – This project was supported by Jiangsu Provincial Health Commission Research Project Approval (No:M2021089).

Authors contributions. – Conceptualization, W.C.W.; investigation, X.C.L., statistical analysis, Z.Y.G., graphics, W.D.S.; writing, original draft preparation, review and editing, Z.J.W. All authors have read and agreed to the published version of the manuscript.

REFERENCES

1. Liu K., Zhao, Wang J, Chen. Y, Zhang. R, Lan. X, Que. J., Etiology, cancer stem cells and potential diagnostic biomarkers for esophageal cancer, *Cancer. Lett.* **8**(28) (2019) 21–28; https://doi.org/10.1016/j.canlet.2019.05.018
2. Baba Y, Nomoto D, Okadome K, Ishimoto T., Iwatsuki M., Miyamoto Y., Yoshida. N, Baba H., Tumor immune microenvironment and immune checkpoint inhibitors in esophageal squamous cell carcinoma, *Cancer Sci.* **111**(9) (2020) 3132–3141;

https://doi.org/10.1111/cas.14541
3. Harada. K, Rogers. JE, Iwatsuki. M, Yamashita. K, Baba. H, Ajani. JA, Recent advances in treating oesophageal cancer, F1000. *Res.* **10**(1) (2020) 1180–11891; https://doi.org/10.12688/f1000research.22926.1
4. Godefa. TM, Derks. S, Thijssen. VLJL,Galectins in Esophageal Cancer: Current knowledge and future perspectives, *Cancers* (Basel) **14**(23) (2022) 5790; https://doi.org/10.3390/CANCERS14235790
5. Thuss-Patience. P, Stein. A, Immunotherapy in squamous cell cancer of the esophagus, Curr. Oncol. **29**(4) (2022) 2461–2471; https://doi.org/10.3390/CURRONCOL29040200
6. Kato. K, Ito. Y, Nozaki. I, Daiko. H, Kojima. T, Yano. M, Ueno. M, Nakagawa. S, Takagi. M, Tsunoda. S, Abe. T, Nakamura. T, Okada. M, Toh. Y, Shibuya. Y, Yamamoto. S, Katayama. H, Nakamura. K, Kitagawa. Y, Japan Esophageal Oncology Group of the Japan Clinical Oncology Group, Parallel-Group Controlled Trial of Surgery Versus Chemoradiotherapy in Patients With Stage I Esophageal Squamous Cell Carcinoma, *Gastroenterology* **161**(6) (2021) 1878–1886; https://doi.org/10.1053/J.GASTRO.2021.08.007
7. Li. R, Zeng. L, Zhao. H, Deng. J, Pan. L, Zhang. S, Wu. G, Ye. Y, Zhang. J, Su. J, Zheng. Y, Deng. S, Bai. R, Zhuang. L, Li. M, Zuo. Z, Lin. D, Zheng. J, Huang. X,ATXN2-mediated translation of TNFR1 promotes esophageal squamous cell carcinoma via m^6A-dependent manner, *Mol. Ther.* **30**(3) (2022) 1089–1103; https://doi.org/10.1016/J.YMTHE.2022.01.006
8. Xu. J, Cao. W, Shao. A, Yang. M, Andoh .V, Ge. Q, Pan. HW, Chen. KP, Metabolomics of esophageal squamous cell carcinoma tissues: Potential biomarkers for diagnosis and promising targets for therapy, *Biomed. Res. Int.* **23** (2022) 7819235; https://doi.org/10.1155/2022/7819235
9. Venkatesh. J, Wasson. MD, Brown. JM, Fernando. W, Marcato. P,LncRNA-miRNA axes in breast cancer: Novel points of interaction for strategic attack, *Cance. Lett.* **7**(1) (2021) 509: 81–88; https://doi.org/10.1016/J.CANLET.2021.04.002
10. Chi. Y, Wang. D, Wang. J, Yu. W, Yang. J, Long non-coding RNA in the pathogenesis of cancers, *Cells* **8**(9) (2021) 1015; https://doi.org/10.3390/cells8091015
11. Lan. Y, Liu. B, Guo. H,The role of M6A modification in the regulation of tumor-related lncRNAs, *Mol. Ther. Nucleic. Acids* **9**(24) (2021) 768–779; https://doi.org/10.1016/J.OMTN.2021.04.002
12. Chen. L, Qiu. CH, Chen. Y, Wang. Y, Zhao. JJ, Zhang. M, LncRNA SNHG16 drives proliferation, migration, and invasion of lung cancer cell through modulation of miR-520/VEGF axis, *Eur. Rev. Med. Pharmacol.* **24**(18) (2020) 9522-9531; https://doi.org/10.26355/EURREV_202009_23037
13. Chen. X, Liu. Y, Sun. D, Sun. R, Wang. X, Li .M, Song. N, Ying. J, Guo. T, Jiang. Y,Long noncoding RNA lnc-H2AFV-1 promotes cell growth by regulating aberrant m6A RNA modification in head and neck squamous cell carcinoma, *Cancer Sci.* **113**(6) (2022) 2071–2084; https://doi.org/10.1111/CAS.15366

14. Xiu. B, Chi. Y, Liu. L, Chi. W, Zhang. Q, Chen. J, Guo. R, Si. J, Li. L, Xue J, Shao. ZM, Wu. ZH, Huang. S, Wu. J, LINC02273 drives breast cancer metastasis by epigenetically increasing AGR2 transcription, *Mol. Cancer* **18**(1) (2019) 187; https://doi.org/10.1186/s12943-019-1115-y
15. Xue. W, Shen. Z, Li. L, Zheng. Y, Yan. D, Kan. Q, Zhao. J,Long non-coding RNAs MACC1-AS1 and FOXD2-AS1 mediate NSD2-induced cisplatin resistance in esophageal squamous cell carcinoma, *Mol. Ther. Nucleic Acids* **10**(23) (2020) 592–602; https://doi.org/10.1016/J.OMTN.2020.12.007
16. Liu. H, Zhang. J, Luo. X, Zeng. M, Xu. L, Zhang. Q, Liu. H, Guo. J, Xu. L, Overexpression of the Long Noncoding RNA FOXD2-AS1 Promotes Cisplatin Resistance in Esophageal Squamous Cell Carcinoma Through the miR-195/Akt/mTOR Axis, *Oncol. Res.* **28**(1) (2020) 65–73; https://doi.org/10.3727/096504019X15656904013079
17. Shi. W, Gao. Z, Song. J, Wang. W, Silence of FOXD2-AS1 inhibited the proliferation and invasion of esophagus cells by regulating miR-145-5p/CDK6 axis, *Histol. Histopathol.* **35**(9) (2020) 1013–1021; https://doi.org/10.14670/HH-18-232
18. Sun. T, Wu. R, Ming. L, The role of m6A RNA methylation in cancer, *Biomed. Pharmacother.* **4**(112) (2019) 108613; https://doi.org/10.1016/j.biopha.2019.108613
19. Ma. S, Chen. C, Ji. X, Liu. J, Zhou. Q, Wang. G, Yuan. W, Kan. Q, Sun. Z,The interplay between m6A RNA methylation and noncoding RNA in cancer, *J. Hematol. Oncol.* **12**(1) (2019) 121; https://doi.org/10.1186/s13045-019-0805-7
20. Rowe. L, Rockwell.AL, Ubiquitous Knockdown of Mettl3 using TRiP.GL01126 Results in Spermatid Mislocalization During Drosophila Spermatogenesis, MicroPub.l Bio. **l7**(18) (2022) 17912–17918; https://doi.org/10.17912/MICROPUB.BIOLOGY.000511
21 Zhou KI, Pan T. Structures of the m(6) A Methyltransferase Complex: Two Subunits with Distinct but Coordinated Roles, *Mol. Cell* **63**(2) (2016) 183–185. doi: 10.1016/j.molcel.2016.07.005
22. Zhou. H, Yin. K, Zhang. Y, Tian. J, Wang. S,The RNA m6A writer METTL14 in cancers: Roles, structures, and applications, *Biochim. Biophys. Acta. Rev. Cancer* **1876**(2) (2021) 188609; https://doi.org/10.1016/J.BBCAN.2021.188609
23. Chen. Z, Zhong. X, Xia. M, Zhong. J, The roles and mechanisms of the m6A reader protein YTHDF1 in tumor biology and human diseases, *Mol. Ther. Nucleic Acids* **26**(9) (2021) 1270–1279; https://doi.org/10.1016/J.OMTN.2021.10.023
24. Li. S, Jiang. F, Chen. F, Deng. Y, Pan. X,Effect of m6A methyltransferase METTL3 -mediated MALAT1/E2F1/AGR2 axis on adriamycin resistance in breast cancer, *J. Biochem. Mol.* Toxico. **l36**(1) (2022) 22922; https://doi.org/10.1002/JBT.22922
25. Chen. H, Yu. Y, Yang. M, Huang. H, Ma. S, Hu. J, Xi. Z, Guo .H, Yao. G, Yang .L, Huang. X, Zhang. F, Tan. G, Wu. H, Zheng. W, Li. L,YTHDF1 promotes breast cancer progression by facilitating FOXM1 translation in an m6A-dependent manner, *Cell. Biosci.* **12**(1) (2022) 19; https://doi.org/10.1186/S13578-022-

00759-W.
26. li jh, liu s, zhou h, qu lh, yang jh. starbase v2.0: decoding mirna-cerna, mirna-ncrna and protein-rna interaction networks from large-scale clip-seq data. nucleic acids res. 2014 jan; 42(database issue): d92-7; https://doi.org/10.1093/nar/gkt1248. epub 2013 dec 1
27. chandrashekar ds, karthikeyan sk, korla pk, patel h, shovon ar, athar m, netto gj, qin zs, kumar s, manne u, creighton cj, varambally s. ualcan: an update to the integrated cancer data analysis platform. neoplasia. 2022 mar; 25:18–27; https://doi.org/10.1016/j.neo.2022.01.001. epub 2022 jan 22.
28. chandrashekar ds, bashel b, balasubramanya sah, creighton cj, ponce-rodriguez i, chakravarthi bvsk, varambally s. ualcan: a
29. Zhou Y, Zeng P, Li YH, Zhang Z & Cui Q (2016) SRAMP: prediction of mammalian N6-methyladenosine (m6A) sites based on sequence-derived features. Nucleic Acids Res. **44**(10) e91.
30. Fan R, Cui C, Kang B, Chang Z, Wang G & Cui Q (2024). A combined deep learning framework for mammalian m6A site prediction, *Cell Genomic* ; https://doi.org/10.1016/j.xgen.2024.100697
31. Tang Z, Li C, Kang B, Gao G, Li C, Zhang Z. GEPIA: a web server for cancer and normal gene expression profiling and interactive analyses, *Nucleic Acids Res.* (2017) Jul 3; 45(W1) :W98-W102; https://doi.org/10.1093/nar/gkx247
32. Cancer Genome Atlas Research Network; Analysis Working Group: Asan University; BC Cancer Agency; Brigham and Women's Hospital; Broad Institute; Brown University; Case Western Reserve University; Dana-Farber Cancer Institute; Duke University; Greater Poland Cancer Centre; Harvard Medical School; Institute for Systems Biology; KU Leuven; Mayo Clinic; Memorial Sloan Kettering Cancer Center; National Cancer Institute; Nationwide Children's Hospital; Stanford University; University of Alabama; University of Michigan; University of North Carolina; University of Pittsburgh; University of Rochester; University of Southern California; University of Texas MD Anderson Cancer Center; University of Washington; Van Andel Research Institute; Vanderbilt University; Washington University; Genome Sequencing Center: Broad Institute; Washington University in St. Louis; Genome Characterization Centers: BC Cancer Agency; Broad Institute; Harvard Medical School; Sidney Kimmel Comprehensive Cancer Center at Johns Hopkins University; University of North Carolina; University of Southern California Epigenome Center; University of Texas MD Anderson Cancer Center; Van Andel Research Institute; Genome Data Analysis Centers: Broad Institute; Brown University:; Harvard Medical School; Institute for Systems Biology; Memorial Sloan Kettering Cancer Center; University of California Santa Cruz; University of Texas MD Anderson Cancer Center; Biospecimen Core Resource: International Genomics Consortium; Research Institute at Nationwide Children's Hospital; Tissue Source Sites: Analytic Biologic Services; Asan Medical Center; Asterand Bioscience; Barretos Cancer Hospital; BioreclamationIVT; Botkin Municipal Clinic; Chonnam National University Medical School; Christiana Care Health System; Cureline;

Duke University; Emory University; Erasmus University; Indiana University School of Medicine; Institute of Oncology of Moldova; International Genomics Consortium; Invidumed; Israelitisches Krankenhaus Hamburg; Keimyung University School of Medicine; Memorial Sloan Kettering Cancer Center; National Cancer Center Goyang; Ontario Tumour Bank; Peter MacCallum Cancer Centre; Pusan National University Medical School; Ribeirão Preto Medical School; St. Joseph's Hospital &Medical Center; St. Petersburg Academic University; Tayside Tissue Bank; University of Dundee; University of Kansas Medical Center; University of Michigan; University of North Carolina at Chapel Hill; University of Pittsburgh School of Medicine; University of Texas MD Anderson Cancer Center; Disease Working Group: Duke University; Memorial Sloan Kettering Cancer Center; National Cancer Institute; University of Texas MD Anderson Cancer Center; Yonsei University College of Medicine; Data Coordination Center: CSRA Inc.; Project Team: National Institutes of Health. Integrated genomic characterization of oesophageal carcinoma, *Nature* **541** (7636) (2017) 169–175; https://doi.org/10.1038/nature20805. Epub 2017 Jan 4.

33. Livak KJ, Schmittgen TD. Analysis of relative gene expression data using real-time quantitative PCR and the 2(-Delta Delta C(T)) *Method. Methods* **25**(4) (2001) 402–408; https://doi.org/10.1006/meth.2001.1262.
34. Ye J, Coulouris G, Zaretskaya I, Cutcutache I, Rozen S, Madden TL. Primer-BLAST: a tool to design target-specific primers for polymerase chain reaction. BMC Bioinformatics. 2012 Jun 18;13:134; https://doi.org/10.1186/1471-2105-13-134
35. Schneider CA, Rasband WS, Eliceiri KW. NIH Image to ImageJ: 25 years of image analysis, *Nat. Methods* **9**(7) (2012) 671–675; https://doi.org/10.1038/nmeth.2089.
36. Cai. J, Chen. Z, Wang. J, Chen. X, Liang. L, Huang. M, Zhang. Z, Zuo. X, CircHECTD1 facilitates glutaminolysis to promote gastric cancer progression by targeting miR-1256 and activating β-catenin/c-Myc signaling, *Cell. Death Dis.* **10**(8) (2019) 576; https://doi.org/10.1038/s41419-019-1814-8
37. Chen. XY, Zhang. J, Zhu. JS,The role of m6A RNA methylation in human cancer, *Mol. Cancer* **18**(1) (2019) 103; https://doi.org/10.1186/s12943-019-1033-z
38. Zhang. C, Liu. J, Guo. H, Hong. D, Ji. J, Zhang. Q, Guan. Q, Ren. Q, m6A RNA methylation regulators were associated with the malignancy and prognosis of ovarian cancer, *Bioengineered* **12**(1) (2021) 3159–3176; https://doi.org/10.1080/21655979.2021.1946305
39. Xue. L, Li. J, Lin. Y, Liu. D, Yang. Q, Jian. J, Peng. J,m^6 A transferase METTL3-induced lncRNA ABHD11-AS1 promotes the Warburg effect of non-small-cell lung cancer, *J. Cell Physiol.* **236**(4) (2012) 2649–2658; https://doi.org/10.1002/jcp.30023
40. Liu. J, Yuan. JF, Wang. YZ, METTL3-stabilized lncRNA SNHG7 accelerates glycolysis in prostate cancer via SRSF1/c-Myc axis, *Exp. Cell Res.* **416**(1) (2022) 113149; https://doi.org/10.1016/J.YEXCR.2022.113149

41. Anita R, Paramasivam A, Priyadharsini JV, Chitra S. The m6A readers YTHDF1 and YTHDF3 aberrations associated with metastasis and predict poor prognosis in breast cancer patients, *Am. J. Cancer Res.* **10**(8) (2020) 2546–2554. PMID: 32905518; PMCID: PMC7471347.
42. Zhang. C, Huang. S, Zhuang. H, Ruan. S, Zhou. Z, Huang. K, Ji. F, Ma. Z, Hou. B, He. X, YTHDF2 promotes the liver cancer stem cell phenotype and cancer metastasis by regulating OCT4 expression via m6A RNA methylation, *Oncogene* **39**(23) (2020) 4507–4518; https://doi.org/10.1038/s41388-020-1303-7